

Simultaneous vibrational resonance in the amplitude and phase quadratures of an optical field based on Kerr nonlinearity

Yinuo Wang, Shan Wu, Cuicui Li, Zhenglu Duan, Min Xie, and Bixuan Fan*
*College of Physics and Communication Electronics,
Jiangxi Normal University, Nanchang 330022, China*

Vibrational resonance (VR) is a nonlinear phenomenon in which the system response to a weak signal can be resonantly enhanced by applying a high-frequency modulation signal with an appropriate amplitude. The majority of VR research has focused on amplifying the amplitude or intensity of the system response to a weak signal, whereas the study of the phase information of system responses in VR remains limited. Here, we investigate the VR phenomena in both amplitude and phase quadratures of an optical field in a Kerr nonlinear cavity driven by a near-resonant weak signal and a far-detuned modulation signal. Analytical and numerical results demonstrated that the resonant enhancement in the amplitude and phase quadratures of the system response to a weak signal simultaneously occurs as the amplitude of the modulation signal is varied. There is a linear relation between the amplitude and frequency of the modulation signal for achieving an optimal VR effect. Furthermore, we generalized our study to investigate the quadrature at an arbitrary phase and determined that the VR enhancement sensitively depends on the phase. Our findings not only broaden the scope of VR research by incorporating phase information but also introduces an approach for amplifying an optical field by manipulating another optical field.

PACS numbers:

I. INTRODUCTION

Resonance refers to the phenomenon by which the amplitude of a physical system at a certain frequency overwhelms that at other frequencies, which commonly occurs in nature, and can be observed or applied in nearly all branches of physics, as well as in many interdisciplinary and engineering fields. Stochastic resonance (SR) is a widely-studied phenomena [3–5, 19, 47], in which noise is utilized to amplify the response of a bistable system to a weak input signal and the optimal amplification or the resonance occurs when the noise-induced average transition rate matches the frequency of the weak signal. SR was first proposed by Benzi et al. in the study of climate change as an enhancement of the response of bistable systems to weak deterministic signals [3–5]. Over time, the study of SR has extended to the various related areas, such as coherence resonance [20, 38, 45], resonant activation [14, 22, 36], noise-induced stability [25, 35, 53], noise-induced pattern formation [12, 41, 43], and noise-enhanced temporal regularity [17, 51].

A noteworthy analogy to SR is vibrational resonance (VR) [31, 33, 50], which occurs when a high-frequency periodic signal replaces noise in SR to amplify the response of a nonlinear system to a weak signal. VR was first numerically observed by Landa and McClintock [33], which was then theoretically [6, 24, 28, 52] and experimentally [2, 8–10] demonstrated in a variety of systems. The study of conventional VR has been extended to a number of variations, that is, aperiodic VR [7, 32], ghost VR [39, 44], nonlinear VR [23, 37], entropic VR [15, 16],

logical VR [26, 27], and vibrational anti-resonance [42]. Owing to the deterministic and controllable nature of VR, it has demonstrated significant potential in several research fields, including weak fault detection [48, 49], weak signal amplification [11, 34], investigating atmospheric disturbance phenomena [30], and bioinformatics [13, 18, 21, 46].

Most of the earlier research regarding VR has focused on the enhancement of the system response to a weak signal, whereas studies regarding the phase information of the system response in the VR phenomena [42] remain limited. In [42], Sarkar and Ray theoretically studied the phase variation of the system response in the vibrational antiresonance phenomenon and demonstrated that a large phase shift was induced by varying the amplitude of a high-frequency field. To the best of our knowledge, the phase properties of the system response to a weak signal in conventional VR has not been investigated thus far. Therefore, in this study, we investigate the VR phenomena in both the amplitude and phase quadratures of an optical signal in the context of a driven single-mode optical cavity containing a Kerr medium. Owing to the self-Kerr interaction of the cavity field, the amplitude and phase quadratures are nonlinearly coupled, providing the basis for studying the VR behaviors in both quadratures. By directly separating the fast and slow motion, we derived the approximate analytical expressions of the response amplitudes for both quadratures. The response amplitude is a typical quantity that can be used to characterize the VR phenomena, which measures the amplitude of the system response at the frequency of the weak signal to be amplified. The results demonstrated that VR simultaneously occurred in the amplitude and phase quadratures as we varied the amplitude of the modulation signal. We also performed numerical simulations to

*Electronic address: fanbixuan@jxnu.edu.cn

verify the analytical results and demonstrated the system dynamics. The numerical results were qualitatively consistent with the analytical results. Notably, the amplitude of the phase quadrature was highly sensitive to the amplitude of the modulation signal in a certain regime, demonstrating the potential to be applied for precision measurements. In addition, the numerical results demonstrated that there was a linear relationship between the modulation amplitude and frequency for the optimal condition of the signal amplification.

In the experiments, the quadrature information of an optical field can be obtained using the standard homodyne detection technique. By adjusting the phase of the local oscillator in the homodyne detection process, the information for the desired quadrature of the system output signal can be acquired. For example, the information of the amplitude and phase quadratures discussed above can be obtained by selecting a phase of zero and $\pi/2$, respectively. To clarify the function of the phase in VR, we numerically investigated the dependence of the response amplitude on the phase of the local oscillator, and the results demonstrated that the response amplitude experienced sine-like oscillations and its maximal value did not correspond to zero or $\pi/2$. Our findings encourage the further investigation of the interplay between VR and the optical phase information, and provide a theoretical guidance for simultaneously amplifying the amplitude and phase quadratures of system responses to a weak optical field by applying another optical field. This may have potential for applications in optical signal detection and energy transfers between optical fields with different frequencies.

In Section II, we introduce the physical model and provide the theoretical formulation. The main results are presented in Section III, including the VR phenomena in the amplitude and phase quadratures of the system response, and the dependence of VR behaviors on the system parameters. Finally, Section IV concludes our study.

II. MODEL AND THEORETICAL ANALYSES

As shown in Fig.1, the model being considered is an anharmonic optical oscillator with a self-Kerr interaction, that is, a single-mode optical cavity containing a nonlinear Kerr medium. The cavity mode is driven by three fields with different frequencies, that is, one driving field (E_d) and two signal fields (E_L and E_H). The Hamiltonian describing the system is expressed by ($\hbar = 1$) as follows:

$$\hat{H} = \omega_c \hat{a}^\dagger \hat{a} + \chi (\hat{a}^\dagger \hat{a})^2 + iE_d (e^{-i\omega_d t} \hat{a}^\dagger - e^{i\omega_d t} \hat{a}) + iE_L (e^{-i\omega_L t} \hat{a}^\dagger - e^{i\omega_L t} \hat{a}) + iE_H (e^{-i\omega_H t} \hat{a}^\dagger - e^{i\omega_H t} \hat{a}). \quad (1)$$

Here, the cavity mode with the resonance frequency ω_c is represented by the annihilation operator \hat{a} . E_d and ω_d are the amplitude and frequency of the driving field, E_L and ω_L are the amplitude and frequency of the low-

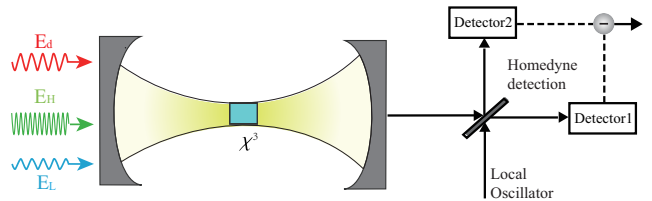


FIG. 1: (Color online) Sketch of our model. A single-mode optical cavity containing a third-order nonlinear Kerr medium is driven by a driving field, E_d , and two signal fields, E_H and E_L . E_L is a weak signal to be amplified and E_H is a modulation signal which is far detuned from the cavity resonance frequency. The output field of the cavity is detected via the homodyne detection.

frequency weak signal, and E_H and ω_H are the amplitude and frequency of the high-frequency modulation signal. χ is the third-order nonlinear coefficient of the Kerr medium. After rotating with respect to the driving frequency ω_d , the Hamiltonian [Eq.(1)] becomes the following:

$$\hat{H} = \Delta \hat{a}^\dagger \hat{a} + \chi (\hat{a}^\dagger \hat{a})^2 + iE_d (\hat{a}^\dagger - \hat{a}) + iE_L (e^{-i\Delta_L t} \hat{a}^\dagger - e^{i\Delta_L t} \hat{a}) + iE_H (e^{-i\Delta_H t} \hat{a}^\dagger - e^{i\Delta_H t} \hat{a}), \quad (2)$$

where the detunings are defined as $\Delta = \omega_c - \omega_d$, $\Delta_L = \omega_L - \omega_d$, and $\Delta_H = \omega_H - \omega_d$. To satisfy the condition of VR, we assume that the two signals have distinguishing frequencies, that is, $\Delta_H \gg \Delta_L$. The corresponding master equation governing the dynamics of the system with the inclusion of the dissipation induced by the interaction with the environment is given by the following:

$$\dot{\rho} = i[\rho, \hat{H}] + \kappa \mathcal{D}[\hat{a}]\rho, \quad (3)$$

where κ is the decay rate of the cavity mode. By using the following relationship $\frac{d}{dt} Tr(\hat{A}\rho) = Tr(\hat{A} \frac{d\rho}{dt})$, we can derive the equation of motion for the mean amplitude of the cavity field as follows:

$$\frac{d\langle \hat{a} \rangle}{dt} = -i(\Delta + \chi) \langle \hat{a} \rangle - \frac{\kappa}{2} \langle \hat{a} \rangle - 2i\chi \langle \hat{a}^\dagger \hat{a}^2 \rangle + E_d + E_L e^{-i\Delta_L t} + E_H e^{-i\Delta_H t}. \quad (4)$$

Under the condition of a weak nonlinearity and strong driving field, we approximately factorized the correlation terms, that is, $\langle \hat{a}^\dagger \hat{a}^2 \rangle \approx \langle \hat{a}^\dagger \rangle \langle \hat{a} \rangle^2$, and defined a classical variable for the mean amplitude of the cavity field $\alpha = \langle \hat{a} \rangle$. The following was then obtained:

$$\frac{d\alpha}{dt} = -(i(\Delta + \chi) + \kappa/2) \alpha - 2i\chi |\alpha|^2 \alpha + E_d + E_L e^{-i\Delta_L t} + E_H e^{-i\Delta_H t}. \quad (5)$$

Note, α is usually a complex variable and therefore Eq.(5) is different from the typical equation of motion in classical nonlinear systems used for investigating the VR phenomena. To transform Eq. (5) into real variables and

make the results experimentally detectable, we defined the amplitude quadrature $x = \frac{\alpha + \alpha^*}{2}$ and phase quadrature $y = \frac{\alpha - \alpha^*}{2i}$, thus the equations of motion of the system can be expressed as follows:

$$\frac{dx}{dt} = -\frac{\kappa}{2}x + (\Delta + \chi)y + 2\chi(x^2 + y^2)y + E_d + E_L \cos \Delta_L t + E_H \cos \Delta_H t, \quad (6)$$

$$\frac{dy}{dt} = -\frac{\kappa}{2}y - (\Delta + \chi)x - 2\chi(x^2 + y^2)x - E_L \sin \Delta_L t - E_H \sin \Delta_H t. \quad (7)$$

Precisely solving the coupled Eqs.(6-7) is complex, as they are differential equations containing nonlinear terms and two driving signals with distinguishing frequencies. Therefore, the slow and fast motions were separated [1, 23, 29, 42]. Thus, the quadrature variables x and y were rewritten as the summation of the slow and fast motions:

$$x(t) = X(t) + \Psi_x(t, \tau = \Delta_H t), \quad (8)$$

$$y(t) = Y(t) + \Psi_y(t, \tau = \Delta_H t). \quad (9)$$

Here, $X(t)$ and $Y(t)$ are the variables characterizing the slow-motion components of the system response caused by F_L , whereas $\Psi_x(t, \tau)$ and $\Psi_y(t, \tau)$ are variables characterizing the fast-motion components caused by F_H , which satisfy

$$\langle \Psi_x(t, \tau) \rangle = \int_0^{2\pi} \Psi_x(t, \tau) d\tau = 0, \quad (10)$$

$$\langle \Psi_y(t, \tau) \rangle = \int_0^{2\pi} \Psi_y(t, \tau) d\tau = 0. \quad (11)$$

By substituting Eqs.(8-9) into Eqs.(6-7) and averaging over one period of the fast motion τ , the following is obtained:

$$\begin{aligned} \frac{dX}{dt} = & -\frac{\kappa}{2}X + (\Delta + \chi)Y + E_d + E_L \cos \Delta_L t \\ & + 2\chi(X^2Y + 2X \langle \Psi_x \Psi_y \rangle + Y^3 + Y \langle \Psi_x^2 \rangle \\ & + 3Y \langle \Psi_y^2 \rangle + \langle \Psi_x^2 \Psi_y \rangle + \langle \Psi_y^3 \rangle), \end{aligned} \quad (12)$$

$$\begin{aligned} \frac{dY}{dt} = & -\frac{\kappa}{2}Y - (\Delta + \chi)X - E_L \sin \Delta_L t \\ & - 2\chi(X^3 + XY^2 + 3X \langle \Psi_x^2 \rangle + X \langle \Psi_y^2 \rangle \\ & + 2Y \langle \Psi_x \Psi_y \rangle + \langle \Psi_x \Psi_y^2 \rangle + \langle \Psi_x^3 \rangle). \end{aligned} \quad (13)$$

Subsequently, the equations for the fast motion can be obtained by subtracting the slow motion Eqs.(12-13) from

the original motion Eqs. (6-7) as follows:

$$\begin{aligned} \frac{d\Psi_x}{dt} = & -\frac{\kappa}{2}\Psi_x + (\Delta + \chi)\Psi_y + E_H \cos \Delta_H t \\ & + 2\chi(X^2\Psi_y + 2XY\Psi_x + 3Y^2\Psi_y + \\ & 2X(\Psi_x\Psi_y - \langle \Psi_x\Psi_y \rangle) + Y(\Psi_x^2 - \langle \Psi_x^2 \rangle) \\ & + 3Y(\Psi_y^2 - \langle \Psi_y^2 \rangle) + \Psi_x^2\Psi_y - \langle \Psi_x^2\Psi_y \rangle + \Psi_y^3 - \langle \Psi_y^3 \rangle) \end{aligned} \quad (14)$$

$$\begin{aligned} \frac{d\Psi_y}{dt} = & -\frac{\kappa}{2}\Psi_y - (\Delta + \chi)\Psi_x - E_H \sin \Delta_H t \\ & - 2\chi(3X^2\Psi_x + 2X(\Psi_x^2 - \langle \Psi_x^2 \rangle) \\ & + Y^2\Psi_x + 2XY\Psi_y + X(\Psi_y^2 - \langle \Psi_y^2 \rangle) \\ & + 2Y\Psi_x\Psi_y - 2Y\langle \Psi_x\Psi_y \rangle + \Psi_x\Psi_y^2 - \langle \Psi_x\Psi_y^2 \rangle) \end{aligned} \quad (15)$$

As Δ_H is assumed to be large, $\dot{\Psi}_x, \dot{\Psi}_y \gg \Psi_x, \Psi_y$, we can obtain the approximate solutions for the fast-motion variables as follows:

$$\Psi_x \approx \frac{E_H}{\Delta_H} \sin \Delta_H t, \quad (16)$$

$$\Psi_y \approx \frac{E_H}{\Delta_H} \cos \Delta_H t. \quad (17)$$

We then obtain $\langle \Psi_x^2 \rangle = \langle \Psi_y^2 \rangle = \frac{E_H^2}{2\Delta_H^2}$ and $\langle \Psi_x \Psi_y \rangle = \langle \Psi_x^2 \Psi_y \rangle = \langle \Psi_x \Psi_y^2 \rangle = 0$. By substituting these approximate solutions for the fast motion into the equations of motion for the slow motion [Eqs. (12-13)], we can obtain the approximate equations merely for the slow motion of the system variables, that is:

$$\begin{aligned} \frac{dX}{dt} = & -\frac{\kappa}{2}X + (\Delta + \chi + \frac{4\chi E_H^2}{\Delta_H^2})Y \\ & + 2\chi(X^2Y + Y^3) + E_d + E_L \cos \Delta_L t, \end{aligned} \quad (18)$$

$$\begin{aligned} \frac{dY}{dt} = & -\frac{\kappa}{2}Y - (\Delta + \chi + \frac{4\chi E_H^2}{\Delta_H^2})X \\ & - 2\chi(X^3 + XY^2) - E_L \sin \Delta_L t. \end{aligned} \quad (19)$$

Eqs.(18-19) demonstrate that the high-frequency signal impacts the steady-state properties of the system by the additional detuning applied to the cavity field.

To evaluate the system response to the weak signal E_L , we first searched for the steady-state solution for X and Y in the absence of the weak signal. The steady-state solution of the field intensity $|\alpha|_s^2$ simply satisfies the following equation:

$$\begin{aligned} 4\chi^2(|\alpha|_s^2)^3 + 4\chi(\Delta + \chi + 4\chi E_H^2/\Delta_H^2)(|\alpha|_s^2)^2 \\ + ((\Delta + \chi)^2 + \kappa^2/4)|\alpha|_s^2 - E_d^2 = 0, \end{aligned} \quad (20)$$

which is a cubic equation of $|\alpha|_s^2$ and can be solved by a standard formula or numerically. From Eqs.(18-19) and the relationship of $|\alpha|_s^2 = X_s^2 + Y_s^2$, we can obtain the steady-state solution of the field Quadratures as follows:

$$Y_s = -\frac{2}{\kappa}(\Delta + \chi + 2\chi|\alpha|_s^2), \quad (21)$$

$$X_s = \frac{E_d}{\kappa/2 - Y_s(\Delta + \chi + 2\chi|\alpha|_s^2)}. \quad (22)$$

Subsequently, we studied the deviation of X and Y from the steady-state solution when a weak signal was applied. Therefore, we expressed X and Y as the summation of their stable solutions and small deviation parts owing to the signal incidence as follows:

$$X = X_s + \delta X, \quad (23)$$

$$Y = Y_s + \delta Y. \quad (24)$$

Here, $(\delta X, \delta Y)$ are the deviations of the system responses (X, Y) from one set of the steady-state solution (X_s, Y_s) .

As the δX and δY deviations were assumed to be small, the nonlinear terms were ignored and the linear equations of motion were obtained for $(\delta X, \delta Y)$:

$$\frac{d\delta X}{dt} = M_{11}\delta X + M_{12}\delta Y + E_L \cos \Delta_L t, \quad (25)$$

$$\frac{d\delta Y}{dt} = M_{22}\delta Y + M_{21}\delta X - E_L \sin \Delta_L t, \quad (26)$$

where $M_{11} = 4\chi X_s Y_s - \frac{\kappa}{2}$, $M_{12} = \Delta + \chi + \frac{4\chi E_H^2}{\Delta_H^2} + 2\chi X_s^2 + 6\chi Y_s^2$, $M_{21} = -(\Delta + \chi + \frac{4\chi E_H^2}{\Delta_H^2} + 6\chi X_s^2 + 2\chi Y_s^2)$, and $M_{22} = -(4\chi X_s Y_s + \frac{\kappa}{2})$. The solutions can be obtained by certain mathematical derivations:

$$\delta X = A \cos(\Delta_L t) + B \sin(\Delta_L t), \quad (27)$$

$$\delta Y = C \cos(\Delta_L t) + D \sin(\Delta_L t). \quad (28)$$

Here, the coefficients are defined as follows:

$$A = \frac{E_L}{C_3} [\Delta_L C_2 M_{22} M_{12} \quad (29)$$

$$+ \Delta_L (\Delta_L M_{12} + C_1) (C_1 M_{11} - M_{21} M_{22} M_{12})],$$

$$B = \frac{1}{C_2} [A (M_{11} C_1 - M_{21} M_{22} M_{12}) \quad (30)$$

$$+ E_L (\Delta_L M_{12} + C_1)],$$

$$C = -\frac{1}{C_1} [A M_{21} M_{22} + \Delta_L (B M_{21} - E_L)], \quad (31)$$

$$D = \frac{A M_{21} + C M_{22}}{\Delta_L}, \quad (32)$$

with $C_1 = \Delta_L^2 + M_{22}^2$, $C_2 = \Delta_L (M_{21} M_{12} + C_1)$, and $C_3 = C_2 M_{21} M_{22}^2 M_{12} - C_1 C_2 (\Delta_L^2 + M_{21} M_{12}) - \Delta_L (M_{11} C_1 - M_{21} M_{22} M_{12}) (C_1 M_{11} - M_{21} M_{22} M_{12})$.

A standard measure of quantitatively characterizing the VR phenomena is the response amplitude Q , which is defined as the ratio between the amplitude of the system response at the signal frequency and amplitude of the input signal. As both quadratures of the cavity field are involved in our model, we evaluated the response amplitudes for the amplitude and phase quadratures as follows:

$$Q_{x,a} = \frac{\sqrt{A^2 + B^2}}{E_L}, \quad (33)$$

$$Q_{y,a} = \frac{\sqrt{C^2 + D^2}}{E_L}. \quad (34)$$

These approximate analytical expressions [Eqs. (33-34)] are the basic results obtained for analyzing the VR behavior in our system.

III. RESULTS AND DISCUSSIONS

Based on the analytical expressions [Eqs.(33)-34], we presented the response amplitudes $Q_{x,a}$ and $Q_{y,a}$ as a function of the modulation amplitude E_H for three different modulation frequencies of $\Delta_H = 200\Delta_L, 500\Delta_L, 800\Delta_L$ [solid curves in Figs.2(a-b)]. All the response amplitudes $Q_{x,a}$ and $Q_{y,a}$ apparently peak at certain values of E_H , indicating the occurrence of VR. As the modulation frequency Δ_H increased, the peak positions of $Q_{x,a}$ and $Q_{y,a}$ tended to shift to larger values of E_H , which is consistent with the results obtained in [23, 40]. This can be explained by Eqs.(18-19), which indicate that the value of E_H^2/Δ_H^2 must be maintained above a certain level to ensure that the high frequency signal has an effective influence on the system. In addition, the peak positions of $Q_{x,a}$ and $Q_{y,a}$ are nearly overlapping in the axis of E_H with the same modulation frequency Δ_H , which implies that VR simultaneously occurs in two quadratures of the system response. Note, the $Q_{y,a}$ curves exhibit a sharp transition, which reveals the high sensitivity of $Q_{y,a}$ to the variation of the controlling parameter E_H .

To verify the validity of the aforementioned approximated analytical results, the equation of motion for α [Eq.(5)] was numerically solved using the fourth-order Runge-Kutta method and the Fourier components of the amplitude and phase quadratures at the characteristic frequency of the weak signal (Δ_L) were computed as follows:

$$Q_{x,s} = \frac{2}{n\pi} \int_0^{nT} x(t) \sin(\Delta_L t), \quad (35)$$

$$Q_{x,c} = \frac{2}{n\pi} \int_0^{nT} x(t) \cos(\Delta_L t), \quad (36)$$

$$Q_{y,s} = \frac{2}{n\pi} \int_0^{nT} y(t) \sin(\Delta_L t), \quad (37)$$

$$Q_{y,c} = \frac{2}{n\pi} \int_0^{nT} y(t) \cos(\Delta_L t), \quad (38)$$

where $T = 2\pi/\Delta_L$ is the period of the weak signal E_L , n is the number of periods of the slow motion determined by the weak signal in the simulation, $Q_{j,s}(j = x, y)$ and $Q_{j,c}(j = x, y)$ represent the sine and cosine components for amplitude and phase quadratures, respectively. Subsequently, the numerical response amplitudes for the two quadratures can be obtained as follows:

$$Q_{x,n} = \frac{\sqrt{Q_{x,s}^2 + Q_{x,c}^2}}{E_L} \quad (39)$$

$$Q_{y,n} = \frac{\sqrt{Q_{y,s}^2 + Q_{y,c}^2}}{E_L} \quad (40)$$

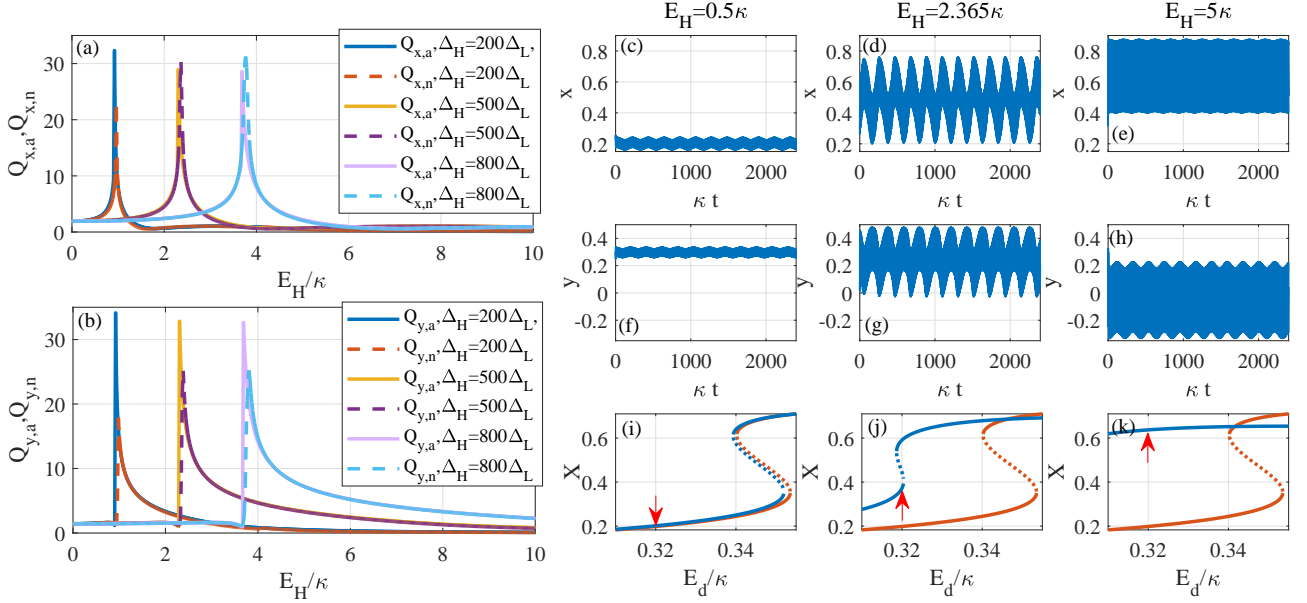


FIG. 2: (Color online) The VR phenomena in both the amplitude and phase quadratures of a weak optical signal by varying the amplitude of the modulation signal E_H . (a-b) Comparison of the analytical and numerical results for the response amplitudes in two quadratures as E_H is varied at three modulation frequencies ($\Delta_H = 200\Delta_L$, $500\Delta_L$, and $800\Delta_L$). The solid curves represent the analytical results $Q_{x,a}$ and $Q_{y,a}$, whereas the dashed curves represent the numerical results $Q_{x,n}$ and $Q_{y,n}$. (c-e) Time evolution of the amplitude quadrature of the cavity field for $E_H = 0.5\kappa$, 2.377κ , 5κ . (f-h) Time evolution of the phase quadrature corresponding to (c-e). (i-k) Stability curves: Steady-state solution of X as a function of the driving amplitude E_d . As labelled by the red arrow, $E_d = 0.32\kappa$ was selected for Figs. 2(a-h). The other parameters were as follows: $\Delta = -2\kappa$, $\chi = \kappa$, $E_L = 0.004\kappa$ and $\Delta_L = 0.03\kappa$.

The value of $Q_{j,n}$ ($j = x, y$) is proportional to the Fourier transform coefficient at $\omega = \Delta_L$, that is, $F_x(\omega) = \int_0^{+\infty} x(t)e^{i\omega t} dt$ or $F_y(\omega) = \int_0^{+\infty} y(t)e^{i\omega t} dt$. The numerical results, $Q_{x,n}$ and $Q_{y,n}$, are indicated by the dashed curves in Fig.2(a). By comparison, the numerical results were apparently qualitatively consistent with the analytical results, demonstrating the validity of the analytical calculations; however, there were certain deviations between the two.

To understand the physical reasons behind the trends of $Q_{x,n}$ and $Q_{y,n}$ as E_H was varied, Figs.2(c-h) present the dynamics of the amplitude and phase quadratures at the three representative points of $E_H = 0.5\kappa$, 2.365κ , 5κ , as well as the corresponding stability curves. For simplicity, $\Delta_H = 500\Delta_L$ was considered for example. When $E_H = 0.5\kappa$, the modulation signal was weak and the system was in the monostable state, as shown in Fig.2(i). Thus, the signals in both quadratures oscillated around the steady-state value with a small amplitude [Fig.2(d,g)], and the amplification of the weak signal was not significant. When E_H was increased to 2.365κ , which is the optimal value for maximizing $Q_{x,n}$ and $Q_{y,n}$ [Fig.2(a-b)], the system became bistable [Fig.2(j)], and the system responses in both quadratures experienced oscillations with notably larger amplitudes [Fig.2(c,f)], resulting in significantly amplified signals at the frequency

of Δ_L . When the amplitude of the high-frequency signal was further increased, that is, $E_H = 5\kappa$, the system became monostable once again [Fig.2(k)] and the low-frequency motion was nearly buried in the strong rapid oscillations [Fig.2(e,h)], which is consistent with the low $Q_{x,n}$ and $Q_{y,n}$ presented in Fig.2(a-b).

To further investigate the detailed dependence of the system responses on the properties of the modulation signal, the response amplitudes of the two quadratures were plotted in the $E_H - \Delta_H$ plane, as shown in Figs.3(a-b), which demonstrated an apparent linear relationship between E_H and Δ_H for achieving resonance. These results are consistent with previous analytical analyses, which demonstrated that the modulation signal modifies the properties of the system stability by the factor of E_H^2/Δ_H^2 . In addition, as E_H was increased from 0 to 4κ , the system responses in the two quadratures gradually increased. However, when $E_H > 4\kappa$, the system response saturated, indicating that an extremely large E_H cannot induce a significant enhancement of the system responses and a moderate modulation signal is adequate for achieving a good VR enhancement.

The output quadrature from homodyne detection apparently relies on the phase of the local oscillator (labelled as ϕ), that is, x and y presented in the preceding section corresponds to $\phi = 0$ and $\phi = \pi/2$, respectively. To generalize our results, the enhancement of the system

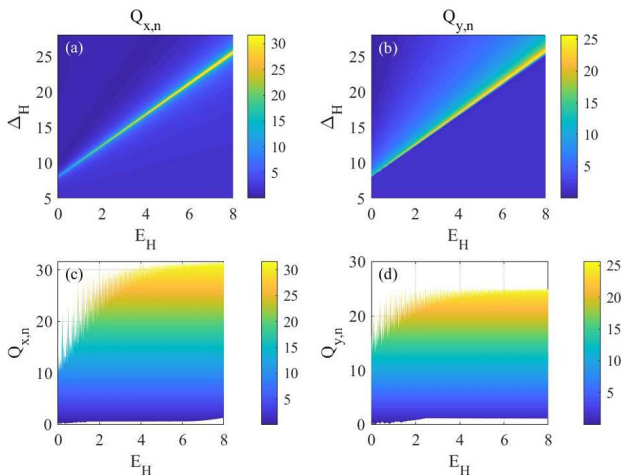


FIG. 3: (Color online) Dependence of the response amplitudes $Q_{x,n}$ and $Q_{y,n}$ on the parameters of the modulation signal (E_H and Δ_H). (a) $Q_{x,n}$ in the E_H - Δ_H plane; (b) $Q_{y,n}$ in the E_H - E_L plane. (c-d) View of the variance of $Q_{x,n}$ and $Q_{y,n}$ versus E_H corresponding to (a-b). The parameters are as follows: $\Delta = -2\kappa$, $\chi = \kappa$, $E_d = 0.32\kappa$, $E_L = 0.004\kappa$, and $\Delta_L = 0.03\kappa$.

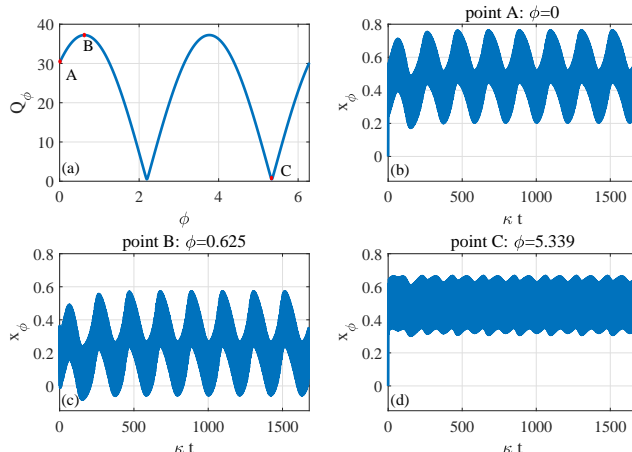


FIG. 4: (Color online) (a) Response amplitude of an arbitrary quadrature x_ϕ versus the phase ϕ . (b-d) Time evolution of x_ϕ at three representative points including A, B, and C in (a). Here, $E_H = 2.365\kappa$, $\Delta_H = 500\Delta_L$, and the other parameters are the same as those shown in Fig.3.

response at the signal frequency of Δ_L for an arbitrary phase in the homodyne detection was studied. In this case, the homodyne signal is expressed as follows:

$$x_{\phi,\text{out}} = \sqrt{\kappa_0} x_\phi = \frac{1}{2}(\alpha_{\text{out}} e^{i\phi} + \alpha_{\text{out}}^* e^{-i\phi}). \quad (41)$$

Here, α_{out} is the amplitude of the output cavity field, which is proportional to the intracavity amplitude α , that

is, $\alpha_{\text{out}} = \sqrt{\kappa_0} \alpha$ ($\sqrt{\kappa_0}$ is the coupling coefficient between the cavity and the homodyne detection device). Thus, we defined the response amplitudes for the quadrature of the phase ϕ as follows:

$$Q_\phi = \frac{\sqrt{Q_{\phi,s}^2 + Q_{\phi,c}^2}}{E_L}, \quad (42)$$

where the sine and cosine Fourier components at the phase ϕ are as follows:

$$Q_{\phi,s} = \frac{2}{n\pi} \int_0^{nT} \frac{1}{2}(\alpha e^{i\phi} + \alpha^* e^{-i\phi}) \sin(\Delta_L t), \quad (43)$$

$$Q_{\phi,c} = \frac{2}{n\pi} \int_0^{nT} \frac{1}{2}(\alpha e^{i\phi} + \alpha^* e^{-i\phi}) \cos(\Delta_L t). \quad (44)$$

As demonstrated in Fig.4(a), the response amplitude Q_ϕ oscillated in a sine-like form as the phase varied from 0 to 2π , indicating that the system response was phase-sensitive. Notably, Q_ϕ did not peak at $\phi = 0$ or $\phi = \pi/2$. Namely, selecting a proper phase of the local oscillator facilitates the signal enhancement effect in VR. To clarify the cause of variation of Q_ϕ , the time evolution x_ϕ of several representative points, including [A: $\phi = 0$ (x quadrature), B: $\phi = 0.625$ (one peak of the Q_ϕ curve), and C: $\phi = 5.339$ (one dip of Q_ϕ curve)], are presented in Figs.4(b-d). At the peak, x_ϕ oscillates at significantly high frequencies associated with a small amplitude of the slow variations, because the varying phase ϕ corresponds to the superposition of the real and imaginary parts of α with different weights. These dynamical behaviors are consistent with the values of Q_ϕ .

IV. CONCLUSION

In this study, the VR phenomenon in a Kerr nonlinear optical cavity with multiple signals was thoroughly analyzed. Contrary to the majority of prior research regarding VR, we incorporated the phase in the investigation of VR. More specifically, we analytically and numerically studied the enhancement in the amplitude and phase quadratures of the system response to a weak low-frequency optical signal by manipulating a high-frequency optical signal. We clarified the optimal parameter regimes required to achieve an effective VR effect. In addition, we generalized our study to an arbitrary quadrature of the system response and found that the system response sensitively relies on the phase of the local oscillator in the homodyne detection. Our study provides a better understanding of the VR mechanism as well as a theoretical guidance for amplifying a weak optical signal by controlling another optical field based on the Kerr nonlinearity.

-
- [1] J. P. Baltanás, L. López, I. I. Blechman, P. S. Landa, A. Zaikin, J. Kurths, and M. A. F. Sanjuán. Experimental evidence, numerics, and theory of vibrational resonance in bistable systems. *Phys. Rev. E*, 67:066119, Jun 2003.
- [2] JP Baltanás, L Lopez, II Blechman, PS Landa, A Zaikin, J Kurths, and MAF Sanjuán. Experimental evidence, numerics, and theory of vibrational resonance in bistable systems. *Physical Review E*, 67(6):066119, 2003.
- [3] Roberto Benzi, Alfonso Sutera, and Angelo Vulpiani. The mechanism of stochastic resonance. *Journal of Physics A: mathematical and general*, 14(11):L453, 1981.
- [4] Roberto Benzi, Giorgio Parisi, Alfonso Sutera, and Angelo Vulpiani. Stochastic resonance in climatic change. *Tellus*, 34(1):10–16, 1982.
- [5] Roberto Benzi, Giorgio Parisi, Alfonso Sutera, and Angelo Vulpiani. A theory of stochastic resonance in climatic change. *SIAM Journal on applied mathematics*, 43(3):565–578, 1983.
- [6] II Blekhman and PS Landa. Conjugate resonances and bifurcations in nonlinear systems under biharmonic excitation. *International Journal of Non-Linear Mechanics*, 39(3):421–426, 2004.
- [7] V. N. Chizhevsky and Giovanni Giacomelli. Vibrational resonance and the detection of aperiodic binary signals. *Phys. Rev. E*, 77:051126, May 2008.
- [8] VN Chizhevsky. Vibrational higher-order resonances in an overdamped bistable system with biharmonic excitation. *Physical Review E*, 90(4):042924, 2014.
- [9] VN Chizhevsky and Giovanni Giacomelli. Experimental and theoretical study of vibrational resonance in a bistable system with asymmetry. *Physical Review E*, 73(2):022103, 2006.
- [10] VN Chizhevsky, Emil Smeu, and G Giacomelli. Experimental evidence of vibrational resonance in an optical system. *Physical review letters*, 91(22):220602, 2003.
- [11] Clerc M.G. Barbay S. et al. Chowdhury, A. Weak signal enhancement by nonlinear resonance control in a forced nano-electromechanical resonator. *Nat. Commun.*, 11: 2400, 2020.
- [12] Debojyoti Das and Deb Shankar Ray. Dichotomous-noise-induced pattern formation in a reaction-diffusion system. *Physical Review E*, 87(6):062924, 2013.
- [13] Bin Deng, Jiang Wang, Xile Wei, KM Tsang, and Wai Lok Chan. Vibrational resonance in neuron populations. *Chaos: An Interdisciplinary Journal of Nonlinear Science*, 20(1), 2010.
- [14] Charles R Doering and Jonathan C Gadoua. Resonant activation over a fluctuating barrier. *Physical review letters*, 69(16):2318, 1992.
- [15] Luchun Du, Ruoshui Han, Jiahao Jiang, and Wei Guo. Entropic vibrational resonance. *Phys. Rev. E*, 102: 012149, Jul 2020.
- [16] Jiang J. H. Yang L. L. Du L. C., Yue W. H. and Ge M. M. Entropic stochastic resonance induced by a transverse driving. *Phil. Trans. R. Soc. A.*, 379:20200228, 2021.
- [17] Bixuan Fan, Xiaomei Wu, and Zhenglu Duan. Enhancement of white-noise-induced temporal regularity in a linear-optical system using coherent feedback. *Phys. Rev. A*, 107:023708, Feb 2023.
- [18] Peng Fu, Can-Jun Wang, Ke-Li Yang, Xu-Bo Li, and Biao Yu. Reentrance-like vibrational resonance in a fractional-order birhythmic biological system. *Chaos, Solitons & Fractals*, 155:111649, 2022.
- [19] Luca Gammaitoni, Peter Hänggi, Peter Jung, and Fabio Marchesoni. Stochastic resonance. *Rev. Mod. Phys.*, 70: 223–287, Jan 1998.
- [20] Hu Gang, T. Ditzinger, C. Z. Ning, and H. Haken. Stochastic resonance without external periodic force. *Phys. Rev. Lett.*, 71:807–810, Aug 1993.
- [21] Mengyan Ge, Lulu Lu, Ying Xu, Rozihajim Mamatimin, Qiming Pei, and Ya Jia. Vibrational mono-/bi-resonance and wave propagation in fitzhugh–nagumo neural systems under electromagnetic induction. *Chaos, Solitons & Fractals*, 133:109645, 2020.
- [22] Pulak Kumar Ghosh and Deb Shankar Ray. A parametric variant of resonant activation: Two-state model approach. *The Journal of chemical physics*, 125(12), 2006.
- [23] Shyamolina Ghosh and Deb Shankar Ray. Nonlinear vibrational resonance. *Physical Review E*, 88(4):042904, 2013.
- [24] M Gitterman. Bistable oscillator driven by two periodic fields. *Journal of Physics A: Mathematical and General*, 34(24):L355, 2001.
- [25] Claudio Guarcello, Davide Valenti, Angelo Carollo, and Bernardo Spagnolo. Stabilization effects of dichotomous noise on the lifetime of the superconducting state in a long Josephson junction. *Entropy*, 17(5):2862–2875, 2015.
- [26] Rong Gui, Yue Wang, Yuangen Yao, and Guanghui Cheng. Enhanced logical vibrational resonance in a two-well potential system. *Chaos, Solitons & Fractals*, 138: 109952, 2020.
- [27] Shengping Huang, Jiacheng Zhang, Jianhua Yang, Houguang Liu, and Miguel AF Sanjuán. Logical vibrational resonance in a symmetric bistable system: Numerical and experimental studies. *Communications in Nonlinear Science and Numerical Simulation*, 119:107123, 2023.
- [28] Akihisa Ichiki, Yukihiro Tadokoro, and Masaki Takanashi. Linear response analysis of vibrational resonance in over-damped systems. *Journal of Physics A: Mathematical and Theoretical*, 45(38):385101, 2012.
- [29] C. Jeevarathinam, S. Rajasekar, and M. A. F. Sanjuán. Theory and numerics of vibrational resonance in duffing oscillators with time-delayed feedback. *Phys. Rev. E*, 83: 066205, Jun 2011.
- [30] A Jeevarekha and P Philominathan. A nonlinear approach to analyse the development of tropical disturbances. *Pramana*, 86:1031–1042, 2016.
- [31] S Jeyakumari, V Chinnathambi, S Rajasekar, and MAF Sanjuan. Single and multiple vibrational resonance in a quintic oscillator with monostable potentials. *Physical Review E*, 80(4):046608, 2009.
- [32] PX Jia, CJ Wu, JH Yang, Miguel AF Sanjuán, and GX Liu. Improving the weak aperiodic signal by three kinds of vibrational resonance. *Nonlinear Dynamics*, 91: 2699–2713, 2018.
- [33] PS Landa and Peter VE McClintock. Vibrational resonance. *Journal of Physics A: Mathematical and general*, 33(45):L433, 2000.
- [34] Guilhem Madiot, Sylvain Barbay, and Rémy Braive.

- Vibrational resonance amplification in a thermo-optic optomechanical nanocavity. *Nano Lett.*, 21:8311–8316, 2021.
- [35] Rosario N. Mantegna and Bernardo Spagnolo. Noise enhanced stability in an unstable system. *Phys. Rev. Lett.*, 76:563–566, Jan 1996. doi: 10.1103/PhysRevLett.76.563.
- [36] M Marchi, F Marchesoni, L Gammaitoni, E Menichella-Saetta, and S Santucci. Resonant activation in a bistable system. *Physical Review E*, 54(4):3479, 1996.
- [37] TLM Djomo Mbong, M Siewe Siewe, and Clément Tchawoua. Controllable parametric excitation effect on linear and nonlinear vibrational resonances in the dynamics of a buckled beam. *Communications in Nonlinear Science and Numerical Simulation*, 54:377–388, 2018.
- [38] Arkady S. Pikovsky and Jürgen Kurths. Coherence resonance in a noise-driven excitable system. *Phys. Rev. Lett.*, 78:775–778, Feb 1997.
- [39] S Rajamani, Shanmuganathan Rajasekar, and Miguel AF Sanjuán. Ghost-vibrational resonance. *Communications in Nonlinear Science and Numerical Simulation*, 19(11):4003–4012, 2014.
- [40] Somnath Roy, Debapriya Das, and Dhruba Banerjee. Vibrational resonance in a bistable van der pol-mathieu-duffing oscillator. *International Journal of Non-Linear Mechanics*, (6):103771, 2021.
- [41] Adolfo Sanz-Anchergues, Anatol M Zhabotinsky, Irving R Epstein, and Alberto P Munuzuri. Turing pattern formation induced by spatially correlated noise. *Physical Review E*, 63(5):056124, 2001.
- [42] Prasun Sarkar and Deb Shankar Ray. Vibrational antiresonance in nonlinear coupled systems. *Physical Review E*, 99(5):052221, 2019.
- [43] G. Stegemann, A. G. Balanov, and E. Schöll. Noise-induced pattern formation in a semiconductor nanostructure. *Phys. Rev. E*, 71:016221, Jan 2005. doi: 10.1103/PhysRevE.71.016221.
- [44] BI Usama, Saverio Morfu, and P Marquie. Vibrational resonance and ghost-vibrational resonance occurrence in chua’s circuit models with specific nonlinearities. *Chaos, Solitons & Fractals*, 153:111515, 2021.
- [45] O. V. Ushakov, H.-J. Wünsche, F. Henneberger, I. A. Khovanov, L. Schimansky-Geier, and M. A. Zaks. Coherence resonance near a hopf bifurcation. *Phys. Rev. Lett.*, 95:123903, Sep 2005.
- [46] Canjun Wang, Keli Yang, and Shixian Qu. Vibrational resonance in a discrete neuronal model with time delay. *International Journal of Modern Physics B*, 28(16):1450103, 2014.
- [47] Thomas Wellens, Vyacheslav Shatokhin, and Andreas Buchleitner. Stochastic resonance. *Reports on Progress in Physics*, 67(1):45, dec 2003.
- [48] Lei Xiao, Xinghui Zhang, Siliang Lu, Tangbin Xia, and Lifeng Xi. A novel weak-fault detection technique for rolling element bearing based on vibrational resonance. *Journal of Sound and Vibration*, 438:490–505, 2019.
- [49] Lei Xiao, Rusmir Bajric, Jingsong Zhao, Junxuan Tang, and Xinghui Zhang. An adaptive vibrational resonance method based on cascaded varying stable-state nonlinear systems and its application in rotating machine fault detection. *Nonlinear Dynamics*, 103:715–739, 2021.
- [50] Chenggui Yao, Yan Liu, and Meng Zhan. Frequency-resonance-enhanced vibrational resonance in bistable systems. *Physical Review E*, 83(6):061122, 2011.
- [51] Danying Yu, Min Xie, Yanbei Cheng, and Bixuan Fan. Noise-induced temporal regularity and signal amplification in an optomechanical system with parametric instability. *Opt. Express*, 26(25):32433–32441, Dec 2018.
- [52] AA Zaikin, L López, JP Baltanás, J Kurths, and MAF Sanjuán. Vibrational resonance in a noise-induced structure. *Physical Review E*, 66(1):011106, 2002.
- [53] Chunhua Zeng, Chun Zhang, Jiakui Zeng, Ruifen Liu, and Hua Wang. Noise-enhanced stability and double stochastic resonance of active brownian motion. *Journal of Statistical Mechanics: Theory and Experiment*, 2015 (8):P08027, 2015.